



LJMU Research Online

Abbas, A, Carnacina, I, Ruddock, F, Alkhaddar, R, Rothwell, G and Andoh, R

The hydraulic performance of the storm chamber in a new manhole designed for separate sewer systems

<http://researchonline.ljmu.ac.uk/id/eprint/12304/>

Article

Citation (please note it is advisable to refer to the publisher's version if you intend to cite from this work)

Abbas, A, Carnacina, I, Ruddock, F, Alkhaddar, R, Rothwell, G and Andoh, R (2020) The hydraulic performance of the storm chamber in a new manhole designed for separate sewer systems. Journal of Hydraulic Research. ISSN 0022-1686

LJMU has developed [LJMU Research Online](#) for users to access the research output of the University more effectively. Copyright © and Moral Rights for the papers on this site are retained by the individual authors and/or other copyright owners. Users may download and/or print one copy of any article(s) in LJMU Research Online to facilitate their private study or for non-commercial research. You may not engage in further distribution of the material or use it for any profit-making activities or any commercial gain.

The version presented here may differ from the published version or from the version of the record. Please see the repository URL above for details on accessing the published version and note that access may require a subscription.

For more information please contact researchonline@ljmu.ac.uk

<http://researchonline.ljmu.ac.uk/>



LJMU Research Online

Abbas, A, Carnacina, I, Ruddock, F, Alkhaddar, R, Rothwell, G and Andoh, R

The hydraulic performance of the storm chamber in a new manhole designed for separate sewer systems

<http://researchonline.ljmu.ac.uk/id/eprint/12304/>

Article

Citation (please note it is advisable to refer to the publisher's version if you intend to cite from this work)

Abbas, A, Carnacina, I, Ruddock, F, Alkhaddar, R, Rothwell, G and Andoh, R (2020) The hydraulic performance of the storm chamber in a new manhole designed for separate sewer systems. JOURNAL OF HYDRAULIC RESEARCH. ISSN 0022-1686

LJMU has developed **LJMU Research Online** for users to access the research output of the University more effectively. Copyright © and Moral Rights for the papers on this site are retained by the individual authors and/or other copyright owners. Users may download and/or print one copy of any article(s) in LJMU Research Online to facilitate their private study or for non-commercial research. You may not engage in further distribution of the material or use it for any profit-making activities or any commercial gain.

The version presented here may differ from the published version or from the version of the record. Please see the repository URL above for details on accessing the published version and note that access may require a subscription.

For more information please contact researchonline@ljmu.ac.uk

<http://researchonline.ljmu.ac.uk/>



The hydraulic performance of the storm chamber in a new manhole designed for separate sewer systems

Journal:	<i>Journal of Hydraulic Research</i>
Manuscript ID	TJHR-2018-0210.R3
Manuscript Type:	Research paper
Date Submitted by the Author:	15-Oct-2019
Complete List of Authors:	Abbas, Alaa; Liverpool John Moores University, Civil Engineering Carnacina, Iacopo; Liverpool John Moores University, Civil Engineering Ruddock, Felicity; Liverpool John Moores University, Civil Engineering Alkhaddar, Rafid ; Liverpool John Moores University, Civil Engineering Rothwell, Glynn; Liverpool John Moores University, Maritime and Mechanical Engineering Andoh, Robert ; AWD Consult Inc.
Keywords:	Dispersion flow, hydraulic structure design, manhole, separated flows, sewer hydraulics
JHR Keywords:	Hydraulic models < Instrumentation, measurements and experimental methods, Flow visualization and imaging < Instrumentation, measurements and experimental methods, Flow-structure interactions < Applied fluid mechanics and hydraulic engineering, Sewer hydraulics < Applied fluid mechanics and hydraulic engineering, Dispersion processes and models < Environmental Fluid Mechanics
Note: The following files were submitted by the author for peer review, but cannot be converted to PDF. You must view these files (e.g. movies) online.	
Full flow 4ls-1-Conventional amnhole.MOV βip over 0.5 - Flow of New Manhole.MOV βip over 0.85 - Flow of New Manhole.MOV βip over 1 - Flow of New Manhole.MOV	

1
2
3
4
5
6
7
8
9
10
11
12
13
14
15
16
17
18
19
20
21
22
23
24
25
26
27
28
29
30
31
32
33
34
35
36
37
38
39
40
41
42
43
44
45
46
47
48
49
50
51
52
53
54
55
56
57
58
59
60



1
2
3
4 The hydraulic performance of the storm chamber in a new manhole designed for
5 separate sewer systems
6
7
8

9 ALAA ABBAS (IAHR Member), Assistant Professor , *Department of Civil Engineering, Liverpool*
10 *John Moores University, Liverpool, United Kingdom*
11 *Email: A.H.Abbas@ljmu.ac.uk (author for correspondence)*
12
13
14

15 IACOPO CARNACINA (IAHR Member), Assistant Professor, *Department of Civil Engineering,*
16 *Liverpool John Moores University, Liverpool, United Kingdom*
17 *Email: I.Carnacina@ljmu.ac.uk (author for correspondence)*
18
19
20

21 FELICITY RUDDOCK, Programme Leader, *Department of Civil Engineering, Liverpool John*
22 *Moores University, Liverpool, United Kingdom*
23 *Email: F.M.Ruddock@ljmu.ac.uk*
24
25
26

27 RAFID ALKHADDAR, Professor of Water and Environmental Engineering, *Head of the Department*
28 *of Civil Engineering, Liverpool John Moores University, Liverpool, United Kingdom*
29 *Email: R.M.Alkhaddar@ljmu.ac.uk*
30
31
32

33 GLYNN ROTHWELL, Assistant Professor, *Department of Maritime and Mechanical Engineering,*
34 *Liverpool John Moores University, United Kingdom*
35 *Email: G.Rothwell@ljmu.ac.uk*
36
37
38

39 ROBERT ANDOH, Professor, *CEO and President of AWD Consult Inc. 100 Tasha Circle,*
40 *Ellenwood, GA 30294, United State of America*
41 *Email: bandoh@awdconsult.com*
42
43
44
45
46
47
48

49 *Running Head: Hydraulic performance of a new manhole*
50
51
52
53
54
55
56
57
58
59
60

1
2
3
4 The hydraulic performance of the storm chamber in a new manhole designed for
5 separate sewer systems
6
7
8
9
10
11

12 **ABSTRACT**
13

14 This paper presents the hydraulic study of a new manhole geometry, designed to allow the installation of
15 separate sewer systems in narrow streets. The new manhole design comprises two chambers in one structure to
16 manage separate flows. The new shape of the manhole generates a new flow pattern for stormwater. It is
17 therefore important to understand the hydraulic properties of sewer systems using the newly designed
18 stormwater manhole chamber. The present study focuses on exploring the hydraulic performance of the storm
19 chamber, which is usually characterized by significant head losses and shockwaves, these related to different
20 flow regimes. A physical model was used to carry out a systematic experiment to explore the flow
21 characteristics of the manhole under both subcritical and transitional flow conditions. The results revealed an
22 enhancement in head loss with higher amplitude waves generated at transition flow when compared with a
23 conventional manhole.
24
25
26
27
28
29
30
31
32

33 *Keywords:* Dispersion flow; hydraulic structure design; manhole; separated flows; sewer
34 hydraulics.
35
36
37
38
39
40
41
42
43
44
45
46
47
48
49
50
51
52
53
54
55
56
57
58
59
60

1 Introduction

A manhole is one of the main elements of the sewer system, making it an important hydraulic structure that influences the hydraulic performance of the entire sewer network. Manholes are used to gain access to the sewer system to carry out cleaning, maintenance and inspection procedures, in addition to aerating the sewer system. They are positioned anywhere between 50 m and 100 m in the system or at any change in inlet or outlet pipe diameter, direction or level (Hager, 2010). Typically, separate sewer systems have two separate manholes: one for storm water flow and one for sewage flow. The sewage flow is easy to predict in comparison to stormwater flow, meaning that more attention needs to be paid to the design of the storm network in order to avoid the risk of flooding. The traditional separate sewer system requires a considerable amount of installation space, this making it a challenge for water companies when dealing with installations in narrow streets, these more common in the UK and EU (Broere, 2016; Marvin & Slater, 1997). A new design for a manhole has been developed in this research to overcome this challenge. The novel manhole includes two chambers: one for sewage flow and one for stormwater flow. The hydraulic performance of the storm chamber in the new manhole design differs from that of the conventional storm manhole for the traditional sewer systems as it generates a new pattern of stormwater flow inside the storm manhole chamber.

Sewers are normally designed to maintain free surface flow conditions using a pipe fill ratio of 85% (Gargano and Hager (2002) recommending 75%), this offering the same discharge capacity of a circular pipe under gravity flow. The flow in a sewer/manhole system is typically subcritical for Froude number (F) < 0.7 , transitional for $0.7 < F < 1.5$ and supercritical for $F > 1.5$ (Hager & Gissoni, 2005), depending on the pipe gradient and flow rate. When the filling ratio of a pipe is β_{ip} = level of water at the inlet of the manhole (h_o)/ inlet pipe diameter (D_p) < 0.5 , there is no shockwave at the outlet of the manhole. The transition, changing $\beta_{ip} > 0.5$, is associated with an interrupted flow which impinges on the outlet manhole (also known as flow choking), and changes the flow from free surface to pressurized air–water flow (Gargano & Hager, 2002). However, designing a storm sewer system with a prescribed filling ratio can be problematic, as there may be difficulties in accurately predicting rainfall intensity and the subsequent average quantity of inlet stormwater to the sewer network. Next to inherent design uncertainties, climate change can further exacerbate the correct design of a stormwater sewer. Transitional and supercritical flows are more common during wet seasons in storm networks or in combined networks. There have been no significant works to develop existing manhole designs, however, there have been many attempts to improve the hydraulic properties of the conventional manhole through the installation of extra accessories to enhance energy dissipation inside the manhole. A non-dissipated, upstream flow energy leads to high downstream flow velocity, this increasing the risk of flooding and erosion while also creating poor operating conditions (Granata, 2016).

1
2
3
4 Granata et al. (2014) investigated the hydraulic performance of drop manholes under
5 supercritical flow conditions. They attempted to improve the hydraulic performance of the
6 conventional drop manhole by installing a dissipative component i.e., two different types of jet-
7 breaker; a plane jet-breaker and a wedge jet-breaker. Other studies have suggested adding control
8 equipment by installing inlet flow restrictors in catchment basins, such as a Vortex Valve, and using
9 these to limit inflow to the hydraulic capacity of the existing combined sewer system (Andoh et al.,
10 2005). Increasing the flow path of storm water, reduces the height of shockwaves in the junction
11 manhole or bend manhole, this associated with an increase in manhole storage capacity. Both these
12 characteristics were identified through experimental tests conducted by Pfister and Gisonni (2014) for
13 the junction manhole, and by Hager and Gisonni (2005) for the bend manhole. Froude number of
14 approach flow (F_o) and filling ratios (β_{ip}) were used as parameters to describe the shockwaves inside
15 the manhole. Saldarriaga et al. (2017) analysed the flow patterns of the symmetric junction in a
16 manhole under supercritical flow conditions, recommending that improving the geometry could
17 subsequently improve the hydraulic performance at the conventional junction manhole.

18
19
20
21
22
23
24
25
26 The new, streamlined manhole design presented in this paper, can improve the performance
27 of a sewer network when compared to previous studies. The design uses a new manhole shape to
28 reduce the footprint of the separate sewer system and to allow the installation of a separate sewer
29 system where space is at a premium. It also increases the storage capacity of the stormwater chamber,
30 extends the path of flow inside the chamber and creates an obstacle to the flow path through the
31 presence of an internal wall. All these features can change the flow pattern of stormwater and increase
32 the dispersion flow energy inside the storm manhole chamber. The subsequent hydraulic performance
33 of the storm chamber in the new manhole was explored and compared with the hydraulic performance
34 of a conventional manhole.

35 36 37 38 39 40 41 42 43 44 *1.1 The new manhole design*

45 The new manhole is cylindrical and has two chambers: the inner chamber is used as the conventional
46 sanitary manhole, the external only used for storm water flow (Abbas et al., 2018). The level of the
47 storm chamber is shallower than the sanitary chamber, the range of depth for both chambers changing
48 according to the level of the inlet/outlet sanitary pipe for the inner chamber and the storm pipe for the
49 outer chamber. In general, it is laid between 1 and 6 m below the road surface. This system requires
50 the storm pipe to be located over the sanitary pipe. The diameter of the sanitary chamber can range
51 from 0.7 to 1 m and the external chamber from 2.1 to 2.5 m, depending on the depth of the manhole.
52 Figure 1 shows the design of the manhole and the separation technique.

2 Physical model

A physical model, an accepted approach used to establish an empirical method for designs or to simulate the flow in the manhole (Crispino et al., 2018), was used to run the experiments. All experiments were carried out in the civil engineering laboratory at Liverpool John Moores University, the aims to: i) explore the energy dispersion of storm flow through the new manhole under different flow rates when compared with the energy dispersion of storm flow through a conventional manhole; ii) to identify the shockwaves produced as a reaction to any alteration of the flow inside the storm chamber and, iii) to determine the velocity distribution at selected points. The physical model to prototype was scaled to 1/5, simulating the new combined manhole shape (Arao et al., 2012). The inner chamber was simulated by a 20 cm diameter Plexiglas pipe, the outer chamber 50 cm in diameter. Both chambers were fixed on one plane base and were 80 cm in length. The inlet pump with a maximum capacity adjustment flow rate of 8.5 l s^{-1} , was set in a water storage tank used to cycle flow water through the system. A flow meter was fixed next to and after the pump to measure the flow rate at a precision of 0.1 l s^{-1} . Two Plexiglas pipes were connected to the manhole's outer chamber as inlet outlet pipes. Both were 10 cm in diameter and 1.5 m in length and equipped with two valves to control the flow rates and depth of flow. Three piezometers were fixed in the system to monitor the decrease in pressure through the model and energy losses. One was at the inlet pipe by the manhole, the second at the outlet pipe, the third at the start point of flow in the pipe after the pump (Fig 2a). A gate valve was placed upstream next to and after the pump to control the water level at the outlet pipe. A second gate valve was placed downstream after the manhole to control the F_o and β_{i_p} at the inlet pipe. A camera was used to record the flow pattern and shockwaves under different flow rates. Two rulers were fixed in the new manhole, one on the external wall, the second on the internal wall to measure the amplitudes of the shockwaves. An OTT Z400 portable instrument, with an accuracy of $\pm 0.01 \text{ m s}^{-1}$, was used to measure the velocity at the inlet and outlet pipes as well as selected points inside the manhole. Head losses were compared with a conventional manhole by removing the inner sanitary chamber and using the external chamber as the conventional storm manhole model at a scale of 1/3. All other tools used for the new manhole are the same as those used to monitor the flow and head losses through the conventional manhole. Figures 2a and 2b show the setup of the physical model for the new manhole design.

2.1 Scale effects

A physical hydraulic model, which is either a smaller or larger scale, simulates the full-scale prototype. This is usually used to test any new design for optimization and investigate the operation

under control conditions in a laboratory (Chanson, 2004). The physical hydraulic model can have scale effects if the scale ratio $\neq 1$. In order to avoid scale effects between a physical scale model and a full-scale prototype, geometric similarity, kinematic similarity and dynamic similarity are required (Heller 2011).

In this study, an undistorted model has been used for the new manhole design. It has geometric similarity in that the same dimensions to scale were used for all components of the model. It also has kinematic similarity as the same direction of flow was used in addition to scale velocity between the physical model and prototype, at each corresponding point. Dynamic similarity requires the same ratios of inertial force to individual force components i.e. the Reynolds number (R_e), F and Weber number (W_e), at corresponding points between the physical model and prototype. This is can only be achieved by using the same scale for both the physical model and prototype or by using different types of fluid in both, neither of which are an economical nor practical solution (Chanson, 2004). As such, Froude similitude, which is more appropriate for modelling a free-surface when the gravity effect is predominant and the flow is highly turbulent, is used in this study. The variation between R_e , which is the inertial force to viscous force, and W_e which is the ratio of inertial force to surface tension between the physical model and the prototype, is associated with scale effects. The scale effects due to surface tension and viscosity can be negligible for the manhole when the $h_o \geq 0.04$ m (Crispino et al., 2018; Pfister and Gisonni, 2014) or when $R_e > 4000$ and W_e is small (Hamill, 2011). Table 1 presents the ranges of dimensionless parameters used to characterize the flow for the physical model of the both manholes. The large-scale ratio (1/5) and turbulent flow in the model reduced these scale effects, this ratio of scale used by many researchers (Arao et al., 2012; Gargano & Hager, 2002; Granata et al., 2011; Stovin et al., 2008; Zhao et al., 2006).

2.2 The test program

Tests were programmed to use a variety of filling ratios (β_{i_p}), starting from 0.25 up to 0.85 for a free-surface, the second set from free surface flow to full flow ($\beta_{i_p} > 1$). Full flow is more common in a combined, or storm, network during heavy rain. The head loss (ΔH), under free-surface conditions and surcharge flow for both manholes, was monitored using dimensional variables such as inlet flow velocity (v), the diameters of both manhole and pipe (D_m and D_p), acceleration due to gravity (g) and the hydraulic gradient along the system (h_f , h_o , h_l and hg).

The head loss (ΔH) under free-surface conditions and surcharge flow for both manholes is mainly dependent on the following dimensional variable when discounting viscosity effects (R_e):

$$\Delta H = f(v, D_m, D_p, h_o, g) \quad (1)$$

The energy loss coefficient (K) is then expressed as a function of non-dimensional, independent variables which represent geometrical ratios as well as force ratios (Arao et al., 2012; Christodoulou, 1991), as shown in the equation below:

$$\frac{\Delta H}{\frac{v^2}{2g}} = f\left(\frac{h_o}{D_m}, \frac{h_o}{D_p}, \frac{v^2}{gh_o}\right) \text{ meaning that } K = f(\beta_{i_m}, \beta_{i_p}, F) \quad (2)$$

where v = mean pipe velocity; g = acceleration due to gravity, D_m = the manhole diameter, D_p = the inlet pipe diameter, h_o = the level of water at the inlet of the manhole, β_{i_p} = the filling ratios of the inlet pipe, β_{i_m} = the surcharge ratio of the manhole and K = the head loss coefficient.

It is assumed that the pipe slope is slight and that the pipe and manhole are circular. The same range of flow rates have been used for both manholes varying between 0.3 and 8.5 l s⁻¹, with an F_o between 0.2 and 0.9. The direct flow used for both manholes was without lateral connection and in total, 154 tests were conducted.

3 Results and discussion

The flow through conventional manholes was described by Hager and Gisonni (2005) who found that shockwaves were generated when the flow was over half the depth of the inlet pipe ($\beta_{i_p} > 0.5$), this further reducing flow energy due to the friction of the flow created by the side walls. Choking occurs at the outlet manhole due to interrupted air-water flow, this resulting in more energy dissipation. Three shockwaves were determined in terms of basic hydraulic quantities for the conventional manhole: two inside the manhole and one at the outlet pipe. A revision of the filling ratio currently used in sewer designs has been recommended by Gargano and Hager (2002) in order for free-surface flow to be maintained at transitional and supercritical flow through the manhole and thus avoid flow choking. Energy flow dissipation inside the sewer manhole is required in many cases, specifically for combined systems or storm networks in a traditional separate sewer system. For example, the drop manhole is used to increase energy dissipation through sewer systems in hilly and mountainous regions for which the F is larger than 1.5 (velocity > 3 m s⁻¹) (Adriana Camino et al., 2014; Granata, 2016; Granata et al., 2011).

The new design of manhole here was designed to increase the head loss of stormwater flow through the storm chamber, in comparison to a conventional storm manhole, and to increase both the storage capacity and retention time of the flow inside the storm chamber. When proposing a new shape of manhole, the need emerges to explore the hydraulic features of the flow inside the new storm chamber and test its hydraulic integrity. Because the sewage water chamber has the same shape as the

conventional manhole in the traditional system, the entire analysis focuses exclusively on the stormwater chamber. This section will first report on the analysis of the head loss coefficient for a different F_o and downstream boundary conditions, then attempt to quantify and study the shockwave amplitude, these results compared with the hydraulic performance of a conventional manhole.

3.1 Head losses through the new manhole

An analytical method was used to determine the head loss (ΔH) of flow inside the manhole from the difference of head pressure between the inlet and outlet of the manhole giving the coefficient of energy loss (Sangster et al., 1958).

$$\Delta H = K \frac{v^2}{2g} \quad (3)$$

The impact of the manhole geometry on the head loss coefficient has been simulated through a number of studies for specific shapes of manhole (Arao et al., 1999). The new manhole design generated a new path for the stormwater flow, as shown in Fig. 2b, where three points were found to disturb the flow and cause head losses in the storm chamber. The first point is the inner chamber wall, which blocks the storm flow path and splits it into two paths (ΔH_w); the second is at the two conduit bends inside the manhole (ΔH_b), the third the expansion and contraction at the entrance and outlet pipes, consequently (ΔH_e) and (ΔH_o).

ΔH_e and ΔH_o are at first approximation, similar to the head losses that occur in the entrance and outlet of the conventional storm manhole; the impact head loss at the entrance was limited by the distance equal to the diameter of the inlet pipe inside the manhole. This study is focused on the other two new head losses, ΔH_w and ΔH_b , generated from the new design of the manhole storm chamber. To simplify the calculation, it is assumed that the entrance and outlet head losses (ΔH_e and ΔH_o) are equal in both manholes, therefore calculated from the measurement of the head loss in a conventional manhole.

The head loss of flow through a conduit bend was investigated by Ito (1960). The head loss coefficient was derived using the ratio of the bend mid-radius, R , and the channel diameter, D , from one side, and the angle of curvature of the bend and the R_e from the other side. Ito's study showed that the minimum head loss coefficient occurred at $R/D = 2$ (Fig. 3), where ζ_k is the head loss as calculated

in Eq. (3). The method used by Ito and the curves extracted from experimental works were applied to the new manhole design to calculate the head loss coefficient of the conduit bend. The new manhole is designed to have relative fixed dimensions between the inner chamber (sewage) and the outer chamber (stormwater) where the R/D ratio is 1.167 and the angle of curvature 45° . The head loss coefficient was found to be approximately 0.1 for the corresponding velocity, equal to 1 m s^{-1} using Ito's (1960) chart. This is expected to be approximately twice that of the head loss coefficient which occurs at the curvature wall of the conventional manhole, as the new manhole design has two bends.

Experimental tests were conducted on both the new and conventional manhole design under the same boundary conditions, to identify the head loss generated from the obstacle to the storm flow path offered by the inner chamber wall (ΔH_w) in the new manhole design. ΔH_e and ΔH_o are the same in both manholes and can be identified from the calculation of the head loss in the conventional manhole. The ΔH_b of the new manhole is approximately twice the ΔH_b at the bend of the conventional manhole. When considering the independent dimensionless parameters for each manhole, Christodoulou (1991) stated that the local head loss in the manhole is essentially dependent on a dynamic parameter in the form of a F expressed in terms of flow velocity, the depth of flow and the geometrical characteristics. The head loss of the manhole is a function of diameter ratio (manhole diameter and pipe diameter) and the shape of the manhole (Pedersen & Mark, 1990). These parameters were used to characterize the hydraulic properties: (1) ratio of surcharge ($\beta_{i_m} = h_o / D_m$), (2) F_o which are simplified by Hager (2010) for a circular channel, see Eq. (4) below, and (3) $\beta_{i_p} = h_o / D_p$

$$F_o = \frac{Q}{\sqrt{gD_p h_o^4}} = \frac{Q}{\sqrt{gD_p^3 \beta_{i_p}^4}} \quad (4)$$

where Q is the water discharge.

The experimental results showed that the flow was subcritical when $F < 0.7$. Free-surface conditions were maintained when the depth of flow was less than 0.5 in the inlet pipe ($\beta_{i_p} = h_o / D_p < 0.5$), changing to flow choking associated with shockwaves, when the flow transitioned from a free-surface to pressurized flow ($\beta_{i_p} > 0.5$).

Figure 4 shows the comparison between the head loss coefficient generated in the new manhole, with the head loss coefficient of the conventional manhole under the same boundary conditions and at a different range of surcharge ratios (β_{i_m}). The data shows a significant increase of flow energy dissipation (increasing in head coefficient) at a low β_{i_m} for the new manhole when

1
2
3
4 compared with the conventional manhole. This difference gradually decreased with an increase in
5 surcharge ratio β_{i_m} in both manholes until the flow transitioned from free-surface flow to pressurized
6 flow, at approximately $\beta_{i_m} = 0.33$ for the new manhole design and $\beta_{i_m} = 0.2$ for the conventional
7 manhole. The head loss coefficient tended to be constant under pressurized flow (full flow). The head
8 loss coefficient of the conventional manhole fluctuates when the flow transfers from free-surface flow
9 to full flow, while the head loss coefficient showed some stability in the new manhole design.
10
11
12
13
14
15

16 The head loss coefficient increases with an increasing filling ratio in the inlet pipe, for both
17 manholes, when the filling ratio was below half the pipe diameter ($\beta_{i_p} < 0.5$), as shown in Fig. 5. The
18 comparison of data head loss coefficients for both manholes at different β_{i_p} , illustrates the tendency of
19 the head loss coefficient to decrease when the filling ratio is $0.5 < \beta_{i_p} < 0.85$, dropping sharply at the
20 transition between free-surface flow and pressurized flow. This coefficient tends to be constant after
21 transitioning from a free-surface to pressurized flow ($\beta_{i_p} > 1$). These results show the same behaviour
22 as the data presented by Arao and Kusuda (1999) for a straight, conventional manhole without drops
23 or changes in direction.
24
25
26
27
28
29
30

31 The head loss coefficient can be correlated to the non-dimensional dynamic momentum
32 component ($F_o \cdot \beta_{i_p}$) to extract preliminary design equations for both manholes. The data presented in
33 Fig. 6, used to simulate the head loss coefficient with a non-dimensional dynamic momentum
34 component, were used to fit Eq. (5), for the new manhole design, and Eq. (6), for the conventional
35 manhole. The application of these two equations is limited to the specific dimension ratio between the
36 inner chamber and external chamber as used in this research.
37
38
39
40
41

$$42 \quad K_{ND} = 0.96(F_o \cdot \beta_{i_p})^{-0.65} \quad (5)$$

$$45 \quad K_0 = 0.75(F_o \cdot \beta_{i_p})^{-0.4} \quad (6)$$

51 *3.2 Shockwaves and choking in the new manhole design*

52 With reference to Hager and Gisonni (2005), shockwaves involve a medium increase of flow depth
53 beyond the shock front, while a hydraulic jump results in the collapse of the supercritical flow regime
54 and a backwater effect. The pattern of flow for conventional manholes was investigated by Gargano
55 and Hager (2002). Different types of waves were identified inside the manhole: i) the small shockwave
56
57
58
59
60

1
2
3
4 resulting from the expansion at the manhole entrance and ii) at the outer manhole the flow impinges on
5 the arc-shaped sides and the top wall, this resulting in a so-called swell wave and choking. The extended
6 experiment in the current research allowed exploration of the main hydraulic features of the new
7 manhole design, including shockwave profiles and variation of velocity. Hereafter, the focus is on the
8 pattern of shockwaves generated from the presence of the inner manhole and changes in the flow path
9 in the stormwater chamber in the new manhole, compared with that in the conventional manhole, for
10 both subcritical and transitional flow conditions.
11
12
13
14

15 In the case of depth ratio $\beta_{i_p} > 0.5$, the impingement of the transitional flow on the manhole
16 wall generates shockwaves associated with swell; the heights and locations of waves in the
17 conventional manhole were determined by Gargano and Hager (2002). The new manhole design
18 presents four shockwave patterns inside the storm chamber, the locations of these shockwaves being
19 A , B , b and C (where C is equivalent to shockwave S in the conventional manhole), as shown in Fig.
20 $2b$.
21
22
23
24
25

26 There are no shockwaves for the subcritical flow ($F < 0.7$) when the filling ratio is below half
27 the inlet pipe ($\beta_{i_p} < 0.5$), as shown in Fig. 7a. The first shockwave (A) appeared when the filling ratio
28 was over $\beta_{i_p} > 0.5$, as shown in Fig. 7b, and continued to be the main shockwave of the flow for $0.5 <$
29 $\beta_{i_p} < 0.85$. This main wave, results from the impingement of the direct flow of the inlet pipe on the
30 inner manhole wall; it is a continuous wave noticed in the new design and associated with transitional
31 flow. The second two symmetrical shockwaves propagated in the storm chamber, B and b , were
32 generated from the change in the flow direction caused by the two bends in the storm chamber. When
33 $0.5 < \beta_{i_p} > 0.85$, these shockwaves were associated with low amplitude. The amplitude of these two
34 shockwaves increased with an increase in β_{i_p} , however, were less than shockwave A when $\beta_{i_p} < 0.85$,
35 as demonstrated in Fig. 7c and Fig. 7d. The generation of these two shockwaves is associated with the
36 swing, or slushing phenomena, for the flow inside the storm chamber. When $\beta_{i_p} > 0.85$, the amplitude
37 of these shockwaves (B and b) increased to be higher than shockwave A , as illustrated in Fig. 7e and
38 $7f$. The characteristics of such waves (B and b) have been described in detail by Hager (2010) with
39 reference to the flow in one bending channel inside a conventional manhole. The last wave, C , was
40 generated from flow choking at the outlet manhole at $\beta_{i_p} > 0.85$, as shown in Fig. 7g. The domain of
41 swirls results from when the choking wave was less than that observed in the conventional manhole,
42 as the B and b shockwaves were predominated on the C wave. The three shockwaves and choking
43 together generate a significant swing wave observed in the storm chamber at transitional flow. Figures
44 $8a$ and $8b$ present the pattern of flow recorded for the conventional manhole where it can be observed
45 that there is no significant shockwave when the filling ratio is less than 0.5 (Fig. 8a). The choking
46
47
48
49
50
51
52
53
54
55
56
57
58
59
60

1
2
3
4 wave (*S*) occurs in the conventional manhole when $0.6 < \beta_{i_p} < 0.75$ (Fig. 8b) as described by Gargano
5 and Hager (2002).
6
7

8
9 The general swing wave generated from the four shockwaves, was used to estimate the
10 characteristic of the average wave amplitude inside the storm chamber of the new manhole design.
11 The relatively high amplitude shockwaves $Y_i = (h_i - h_1) / h_1$, which vary with the non-dimensional
12 dynamic momentum $F_o \beta_{i_p}$, are used to quantify the pattern of shockwaves, where h_i is the wave
13 amplitude observed in the manhole (Gargano & Hager, 2002). Figure 9 illustrates the Y_i over $(F_o \beta_{i_p})$
14 relationship for both the conventional and new manhole. The experimental results illustrate how high
15 amplitude shockwaves increase rapidly when the flow changes from free-surface flow to pressurized
16 flow; the conventional manhole has smaller amplitude shockwaves. The main shockwave (choking
17 wave) normally occurs at the transitions between free-surface flow and pressurized flow for the
18 conventional manhole and increases with increased dynamic momentum. The swing of the waves
19 recorded in the conventional manhole was less than in the new manhole design and attained a
20 maximum $F_o \beta_{i_p} > 0.5$. This then became constant for larger values of $F_o \beta_{i_p}$ as the wave transitioned
21 from 0.1 to 0.05 (De Martino, 2002). The fluctuation range and the location of the choking wave
22 recorded in these experiments for similar β_{i_p} , was comparable to the shockwave *S*, identified by
23 Gargano and Hager (2002), in the conventional manhole. These relationships were quantified for both
24 manholes using Eq. (7) for the new manhole and Eq. (8) for the conventional manhole.
25
26
27
28
29
30
31
32
33

$$34 \quad Y_{i(ND)} = 0.12 \ln(F_o \beta_{i_p}) + 0.32 \quad (7)$$

$$35 \quad Y_{i(o)} = 0.03 \ln(F_o \beta_{i_p}) + 0.09 \quad (8)$$

36
37
38
39
40
41
42
43 The high swing amplitude associated with the transitional flow in the new manhole design
44 can cause damage to the manhole structure and decrease the hydraulic capacity of the manhole. As
45 such, it is an important design parameter to be considered. The shockwaves generated increase the
46 flow depth beyond the shock front. This phenomenon causes a decrease in discharge capacity and
47 may result in geysering of storm water out of the manhole onto the street (Hager & Gisonni, 2005).
48 Therefore, the experimental work was extended using the physical model, to test the amplitude of
49 shockwaves when a breakdown occurs in the flow downstream of the model. The gate valve located
50 downstream of the physical model (the valve after the manhole), was used to disturb the flow and
51 generate a backwater effect. This data provides a better understanding of manhole flow behaviour and
52 tests the hydraulic integrity of the new manhole.
53
54
55
56
57
58
59
60

1
2
3
4 The surcharge ratio (βi_m) of the new manhole and the conventional manhole can also be
5 related to the amplitude of the shockwaves at a fixed flow rate and for a variety of flow rates at
6 transitional flow. Figure 10 illustrates the impact of the surcharge ratio (βi_m) on the amplitudes of the
7 shockwaves (Y_i) for the new manhole design. Maximum Y_i were observed generally at a low
8 surcharge ratio for the transitional flow. The wave amplitudes decreased until close to zero, when the
9 surface water level in the manhole was stable, with an increase of surcharge ratio (βi_m). The amplitude
10 and swing of shockwaves are around zero when the surcharge ratio is approximately equal to the
11 diameter of manhole D_m (surcharge ratio $\beta i_m = 1$). A reduction in shockwaves provides an appropriate
12 safety factor to avoid high hydrostatic pressure loads inside the manhole generated from the swing of
13 the wave at a high surcharge ratio, although this may create pressure flow conditions within the
14 network. The storm chamber in the new manhole has a higher storage capacity and longer path for
15 stormwater flow compared with the conventional stormwater manhole. The retention time results
16 from the extended path of stormwater flow and an increase in the storm system upstream, improving
17 the hydraulic performance of the storm network and decreasing flooding risks downstream of the
18 network.
19
20
21
22
23
24
25
26
27
28
29
30
31
32
33
34

35 **4 Conclusion**

36 This research explored the hydraulic performance of a novel manhole design, focusing exclusively on
37 the storm chamber. The novel shape of the manhole was designed to facilitate the installation of
38 separate sewer systems in narrow streets which are prevalent in UK and EU cities. Experimental
39 works were conducted to explore and quantify the hydraulic properties of the flow through the new
40 storm chamber, comparing this with that of a conventional manhole. The head loss coefficient and the
41 pattern of shockwaves were investigated for both manholes under the same conditions using the
42 independent dimensionless parameters for each manhole: ratio of surcharge (βi_m), approach flow
43 Froude numbers (F_o), and filling ratios (βi_p). The new manhole design generates higher head losses,
44 about twice the head loss generated in a conventional manhole, at a low βi_m . The head loss for both
45 manholes tends to be stable and maintains a lower constant value when the flow transitions from free-
46 surface flow to pressurized flow (at high βi_m). The domains of generating the head loss for the flow
47 inside the storm chamber were determined; the inner chamber wall, the two conduit bends inside the
48 manhole and the expansion and contraction at the entrance and outlet pipes. Four shockwaves were
49 identified in the storm chamber of the new manhole design: (1) Shockwave A results from
50 impingement of the direct flow of the inlet pipe on the inner manhole wall; (2 & 3) B and b were
51
52
53
54
55
56
57
58
59
60

1
2
3
4 generated from the change in the flow direction caused by the two bends in the storm chamber and (4)
5 shockwave C was generated from flow choking at the outlet manhole. The locations of these
6 shockwaves were determined and the average amplitude of swing generated from the combined
7 effects of these shockwaves quantified with non-dimensional dynamic momentum $F_o \beta_{i_p}$. The results
8 showed a significant increase in shockwave amplitude in the new manhole design when the flow
9 changed from free-surface to pressurise flow, this increasing the risk of failure in manhole
10 performance. Therefore, the hydraulic integrity of the storm chamber in the new manhole was tested
11 by breaking up the flow downstream of the model. The experimental results illustrated that the
12 amplitude and swing of shockwaves decreases with an increase in the surcharge ratio (β_{i_m}), this
13 suggesting that the manhole design is safe in terms of structural damage and geysering phenomena
14 associated risks. The study used a fixed dimensions ratio between the inner and outer chambers, and
15 one coaxial configuration of the inner manhole located inside the outer chamber. The research can be
16 developed to test a full-scale manhole insitu which allows to measure the scale effects on the flow
17 properties and to develop a computational fluid dynamic model (CFD) to explore different
18 configurations of the new manhole design.
19
20
21
22
23
24
25
26
27
28
29
30

31 **Acknowledgements:**

32
33 The authors would like to acknowledge the United Utilities Group PLC for providing technical
34 support. The first author would like to acknowledge Al Ghalowa Co Ltd. for supporting this study. A
35 special acknowledgement is for the technical staff of LJMU for their assistance with the experimental
36 set-up.
37
38
39
40
41
42
43
44

45 **Funding:**

46
47 There has been no significant financial support for this work that could have influenced its outcome.
48
49
50

51 **Supplemental data**

52
53 This paper included supplemental material. Video clips show flow patterns and shockwaves generated
54 at each corresponding flow rate for the new manhole design and for the conventional manhole.
55
56
57
58
59
60

Notation

A, B, b and C = shockwaves generated in the new manhole (-)

D_m = manhole diameter (m)

D_p = approach pipe diameter (m)

F = Froude number (-)

F_o = approach Froude number (-)

$F_o \beta_{ip}$ = non-dimensional dynamic momentum component

g = gravity acceleration (m s^{-2})

h_f = level of water at the beginning of inlet pipe (m)

h_g = level of water at the outlet of manhole (m)

h_i = level of amplitude of water in the manhole (m)

h_l = level of water in the manhole (m)

h_o = level of water at inlet of the manhole (m)

K_o = head loss coefficient (-), K_{ND} for the new manhole design and K_o for the conventional manhole

Q = discharge ($\text{m}^3 \text{s}^{-1}$)

R = the bend mid-radius (m)

Re = Reynolds number (-)

S and E = shockwaves generated in the conventional manhole (-)

Y_i = shockwaves amplitudes (-), $Y_{i(ND)}$ for the new manhole design and $Y_{i(o)}$ for the conventional manhole.

β_{im} = ratio of surcharge for the manhole (-)

β_{ip} = filling ratio in the approach pipe (-)

ΔH = head loss (m)

v = mean pipe velocity (m s^{-1})

We = Weber number (-)

References

- Abbas, A., Ruddock, F., Al Khaddar, R., Rothwell, G., & Andoh, R. (2018). Improving the Geometry of Manholes Designed for Separate Sewer Systems. *Canadian Journal of Civil Engineering*, , 46(1), 13-25.
- Adriana Camino, G., Zhu, D. Z., & Rajaratnam, N. (2014). Flow observations in tall plunging flow dropshafts. *Journal of Hydraulic Engineering*, 141(1), 06014020.
- Andoh, R. Y. G., Stephenson, A. J., & Collins, P. (2005). Approaches to Urban Drainage Systems Management for The 21 st Century. In *National Hydrology Seminar*.
- Arao, S., Kusuda, T., Moriyama, K., Hiratsuka, S., Asada, J., & Hirose, N. (2012). Energy losses at three-way circular drop manholes under surcharged conditions. *Water Science and Technology*, 66(1), 45-52.
- Arao, S., Mihara, T., & Kusuda, T. (1999). An optimal design method of storm sewer network considered with manhole energy loss. *Doboku Gakkai Ronbunshu*, 1999(614), 109-120.
- Broere, W. (2016). Urban underground space: Solving the problems of today's cities. *Tunnelling and Underground Space Technology*, 55, 245-248.
doi:<https://doi.org/10.1016/j.tust.2015.11.012>
- Chanson, H. (2004). *Hydraulics of open channel flow*: Elsevier.
- Christodoulou, G. C. (1991). Drop manholes in supercritical pipelines. *Journal of Irrigation and Drainage Engineering*, 117(1), 37-47.
- Crispino, G., Pfister, M., & Gissonni, C. (2019). Supercritical flow in junction manholes under invert-and obvert-aligned set-ups. *Journal of Hydraulic Research*, , 57(4), 534-546.

- 1
2
3
4 Gargano, R., & Hager, W. H. (2002). Supercritical Flow across Sewer Manholes. *Journal of*
5
6 *Hydraulic Engineering*, 128(11), 1014-1017. doi:10.1061/(ASCE)0733-
7
8 9429(2002)128:11(1014)
9
10
11 Granata, F. (2016). Dropshaft cascades in urban drainage systems. *Water Science and*
12
13 *Technology*, 73(9), 2052-2059.
14
15
16 Granata, F., De Marinis, G., & Gargano, R. (2014). Flow-improving elements in circular drop
17
18 manholes. *Journal of Hydraulic Research*, 52(3), 347-355.
19
20 doi:10.1080/00221686.2013.879745
21
22
23 Granata, F., de Marinis, G., Gargano, R., & Hager, W. H. (2011). Hydraulics of Circular
24
25 Drop Manholes. *Journal of Irrigation & Drainage Engineering*, 137(2), 102-111.
26
27 doi:10.1061/(ASCE)IR.1943-4774.0000279
28
29
30 Hager, W. H. (2010). *Wastewater Hydraulics Theory and Practice*. Springer Science &
31
32 Business Media.
33
34
35 Hager, W. H., & Gisonni, C. (2005). Supercritical flow in sewer manholes. *Journal of*
36
37 *Hydraulic Research*, 43(6), 660-667. doi:10.1080/00221680509500385
38
39
40 Hamill, L. (2011). *Understanding hydraulics*. Macmillan International Higher Education.
41
42
43 Ito, H. (1960). Pressure losses in smooth pipe bends. *Journal of Basic Engineering*, 82(1),
44
45 131-140.
46
47
48 Marvin, S., & Slater, S. (1997). Urban infrastructure: the contemporary conflict between
49
50 roads and utilities. *Progress in Planning*, 4(48), 247-318.
51
52
53 Pedersen, F. B., & Mark, O. (1990). Head losses in storm sewer manholes: submerged jet
54
55 theory. *Journal of Hydraulic Engineering*, 116(11), 1317-1328.
56
57
58 Pfister, M., & Gisonni, C. (2014). Head losses in junction manholes for free surface flows in
59
60 circular conduits. *Journal of Hydraulic Engineering*, 140(9), 06014015.

- 1
2
3
4 Saldarriaga, J., Rincon, G., Moscote, G., & Trujillo, M. (2017). Symmetric junction manholes
5 under supercritical flow conditions. *Journal of Hydraulic Research*, 55(1), 135-142.
6
7 doi:10.1080/00221686.2016.1212410
8
9
10
11 Sangster, W. M., Wood, H. W., Smerdon, E. T., & Bossy, H. G. (1958). Pressure changes at
12 storm drain junctions.
13
14
15 Stovin, V. R., Guymer, I., & Lau, S. D. (2008, August). Approaches to validating a 3D CFD
16 manhole model. In *11th international conference on urban drainage* (pp. 1-10).
17
18
19
20 Zhao, C.-H., Zhu, D. Z., & Rajaratnam, N. (2006). Experimental Study of Surcharged Flow
21 at Combining Sewer Junctions. *Journal of Hydraulic Engineering*, 132(12), 1259-
22
23 1271. doi:10.1061/(ASCE)0733-9429(2006)132:12(1259)
24
25
26
27
28
29
30
31
32
33
34
35
36
37
38
39
40
41
42
43
44
45
46
47
48
49
50
51
52
53
54
55
56
57
58
59
60

1
2
3
4 **List of tables**
5

6 Table 1 Experimental range of main dimensionless parameters.
7
8
9
10
11
12
13
14
15
16
17
18
19
20
21
22
23
24
25
26
27
28
29
30
31
32
33
34
35
36
37
38
39
40
41
42
43
44
45
46
47
48
49
50
51
52
53
54
55
56
57
58
59
60

List of figures

Figure 1 3D design of the innovative manhole.

Figure 2 The physical model used to test the hydraulic properties for the new manhole design (a) a cross section (b) a top view showing the location of shockwaves.

Figure 3 Total loss coefficient as a function of relative bend radius R/D and angles of curvature δ for $Re \geq 10^6$ (Hager, 2010).

Acknowledgements: Reprinted by permission from [Springer Nature]: (Wastewater Hydraulic Book, Losses in Flow chapter, Willi H. Hager, 2010).

Figure 4 A comparison between the head loss of the new manhole design and conventional manhole at different surcharge ratios (β_{i_m}).

Figure 5 A comparison between the head loss coefficient of the new manhole design and the conventional manhole at different filling ratios (β_{i_p}).

Figure 6 Relationship between the head loss coefficient and the non-dimensional dynamic momentum component ($F_o \cdot \beta_{i_p}$) for the new manhole design and the conventional manhole.

Figure 7 The pattern of shockwaves generated in the new manhole design at different filling ratios (β_{i_p}) (a) No significant shockwave noticed when the filling ratio $\beta_{i_p} < 0.5$ (b) The first and main shockwave A appeared when $\beta_{i_p} > 0.5$ (c) The second shockwave B associated with A appeared when $0.5 < \beta_{i_p} < 0.85$, but A is still the main shockwave (d) Swing phenomena appeared when $0.5 < \beta_{i_p} < 0.85$ (e) Shockwave B and b are larger than shockwave A when $\beta_{i_p} > 0.85$ (f) Shockwave B and b are larger than shockwave A when $\beta_{i_p} > 0.85$ is associated with an increase in the swing phenomena (g) Shockwave B and b are larger than shockwave A when $\beta_{i_p} > 0.85$.

Figure 8 The pattern of shockwaves generated in the conventional manhole design at different filling ratios (β_{i_p}) (a) The flow pattern for the conventional manhole under filling ratio $\beta_{i_p} < 0.5$: there is no shockwave (b) The flow pattern for the conventional manhole under filling ratio $\beta_{i_p} > 0.5$: shockwave S is generated.

Figure 9 The amplitude of the average shockwaves (Y_i) against non-dimensional dynamic momentum ($F_o \cdot \beta_{i_p}$) for both the conventional and the new manhole design.

1
2
3
4 Figure 10 The wave amplitude (Y_i) at different surcharge ratios (βi_m) for the flow in the new manhole
5
6 design at different flow rates.
7
8
9
10
11
12
13
14
15
16
17
18
19
20
21
22
23
24
25
26
27
28
29
30
31
32
33
34
35
36
37
38
39
40
41
42
43
44
45
46
47
48
49
50
51
52
53
54
55
56
57
58
59
60

Table 1. Experimental range of main dimensionless parameters

Manhole	βi_m	βi_p	F_o	R_e		W_e	
				model	prototype	model	prototype
New design	0.1 – 0.5	0.3 – 1.5	0.25 – 0.9	9500 - 71500	21500 -167000	0.1 - 0.9	0.4 - 5.0
Conventional	0.05 – 0.3	0.2 – 1.3	0.4 – 0.9	15000 - 72000	34000 - 180000	0.2 - 1.0	0.7-5.0

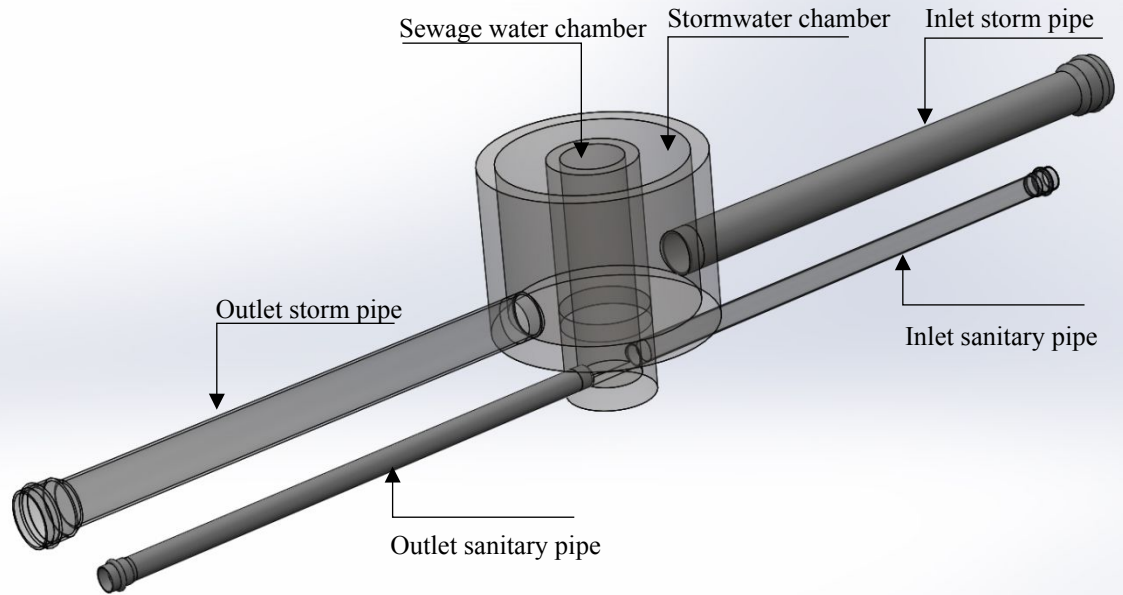


Figure 1 3D design of the innovative manhole.

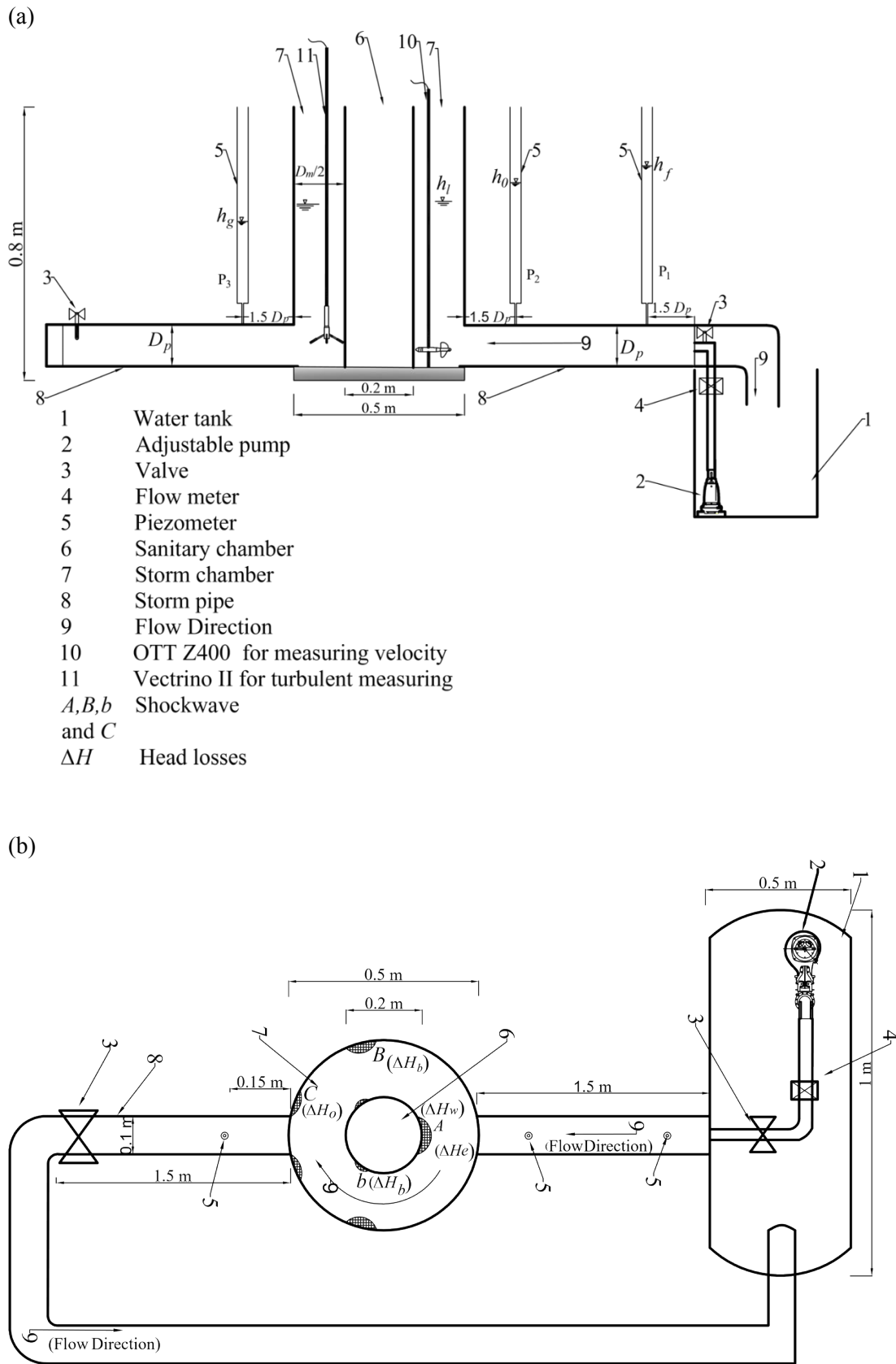


Figure 2 The physical model to test the hydraulic properties for the new manhole design (a) a cross section (b) a top view shows the location of shockwaves.

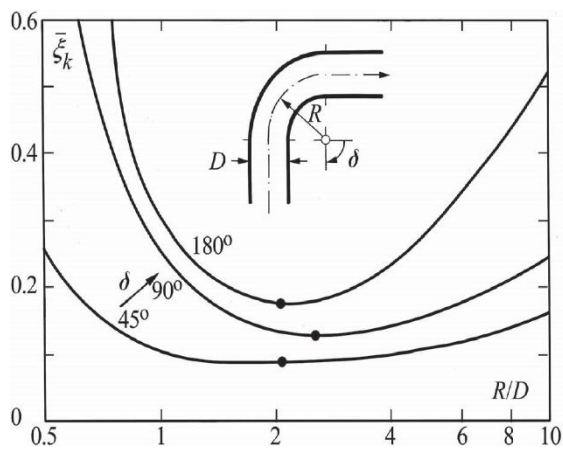


Figure 3 Total loss coefficient as a function of relative bend radius R/D and angles of curvature δ for $Re \geq 10^6$ (Hager, 2010).

Acknowledgements: Reprinted by permission from [Springer Nature]: (Wastewater Hydraulic Book, Losses in Flow chapter, Willi H. Hager, 2010).

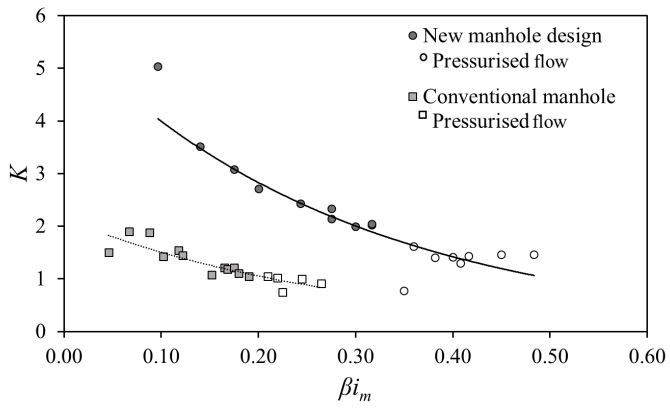


Figure 4 A comparison between the head loss of the new manhole design and conventional manhole at different surcharge ratio (βi_m).

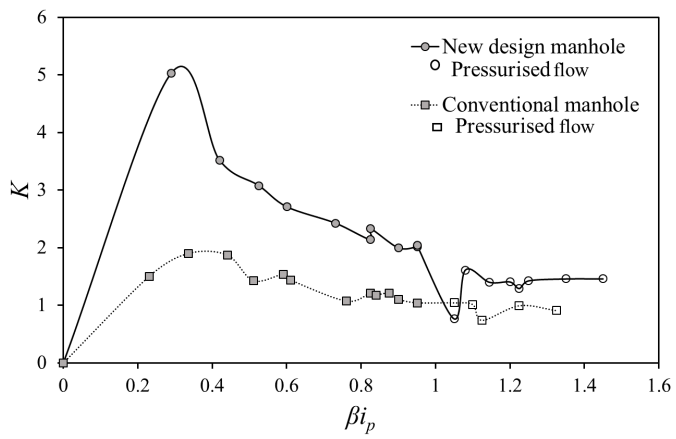


Figure 5 A comparison between the head loss of the new manhole design and the conventional manhole at different filling ratios (βi_p).

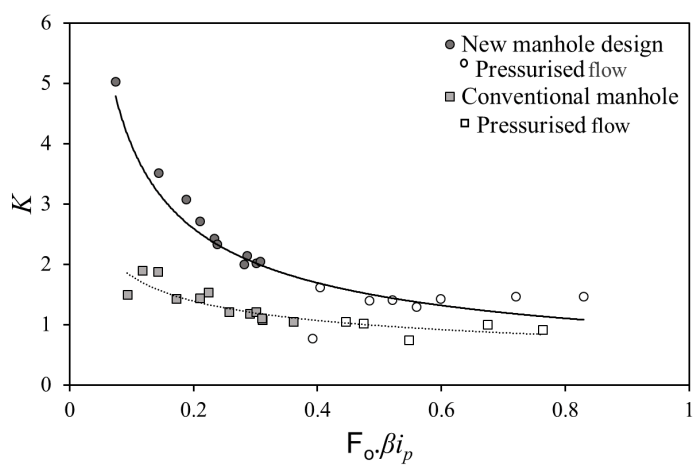


Figure 6 Relationship between the head loss coefficient and the non-dimensional dynamic momentum component ($F_o \beta i_p$) for the new manhole design and the conventional manhole.

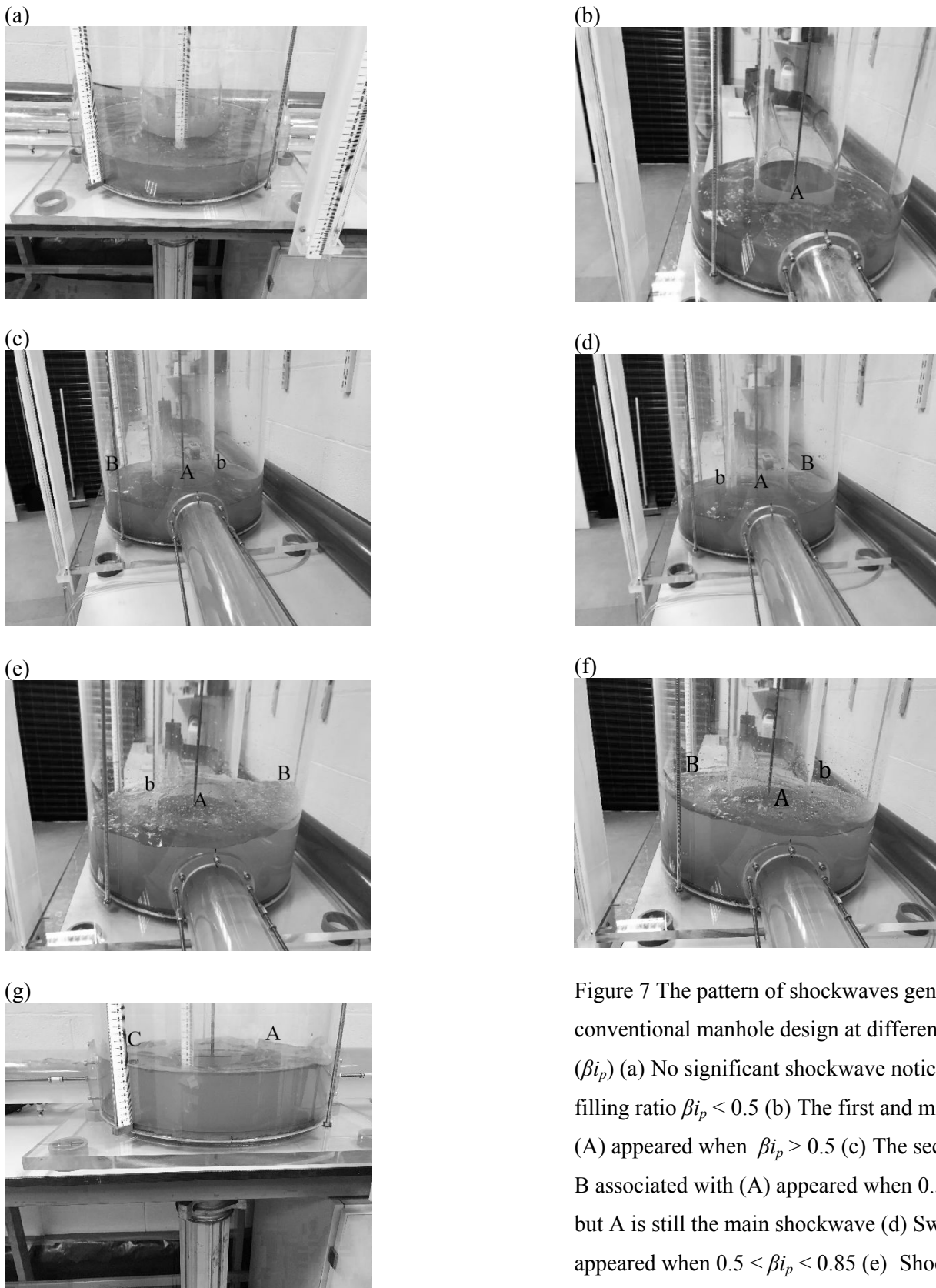


Figure 7 The pattern of shockwaves generated in the conventional manhole design at different filling ratios (β_{i_p}) (a) No significant shockwave noticed when the filling ratio $\beta_{i_p} < 0.5$ (b) The first and main shockwave (A) appeared when $\beta_{i_p} > 0.5$ (c) The second shockwave B associated with (A) appeared when $0.5 < \beta_{i_p} < 0.85$, but A is still the main shockwave (d) Swing phenomena appeared when $0.5 < \beta_{i_p} < 0.85$ (e) Shockwave B and b are larger than shockwave A when $\beta_{i_p} > 0.85$ (f) Shockwave B and b are larger than shockwave A when $\beta_{i_p} > 0.85$ is associated with an increase in the swing phenomena (g) Shockwave B and b are larger than shockwave A when $\beta_{i_p} > 0.85$.

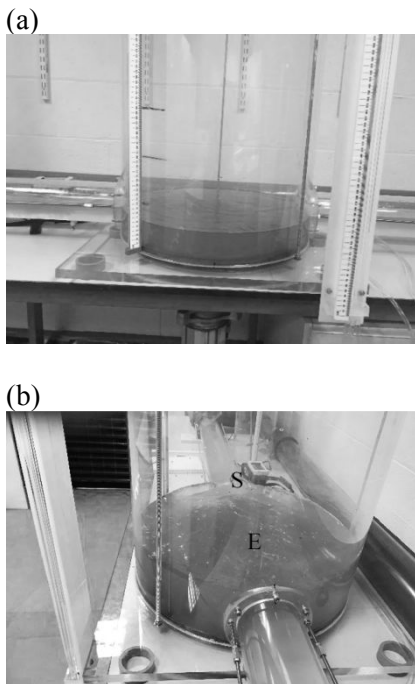


Figure 8 The pattern of shockwaves generated in the conventional manhole design at different filling ratios (β_{i_p}) (a) The flow pattern for the conventional manhole under filling ratio $\beta_{i_p} < 0.5$: there is no shockwave (b) The flow pattern for the conventional manhole under filling ratio $\beta_{i_p} > 0.5$: shockwave S is generated.

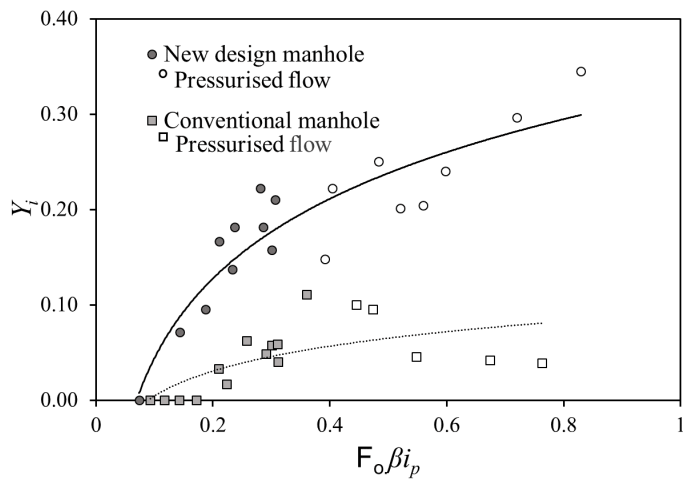


Figure 9 The amplitude of the average shockwaves (Y_i) against non-dimensional dynamic momentum ($F_o \beta i_p$) for both the conventional and the new manhole design.

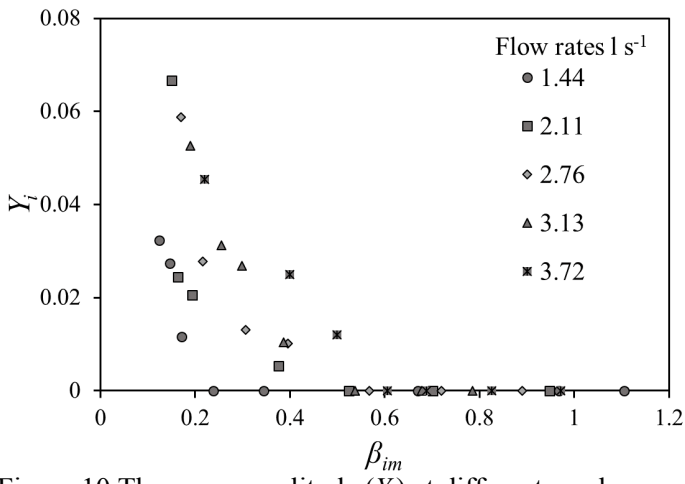


Figure 10 The wave amplitude (Y_i) at different surcharge ratios (β_{im}) for the flow in the new manhole design at different flow rates.

1
2
3
4
5
6
7
8
9
10
11
12
13
14
15
16
17
18
19
20
21
22
23
24
25
26
27
28
29
30
31
32
33
34
35
36
37
38
39
40
41
42
43
44
45
46
47
48
49
50
51
52
53
54
55
56
57
58
59
60

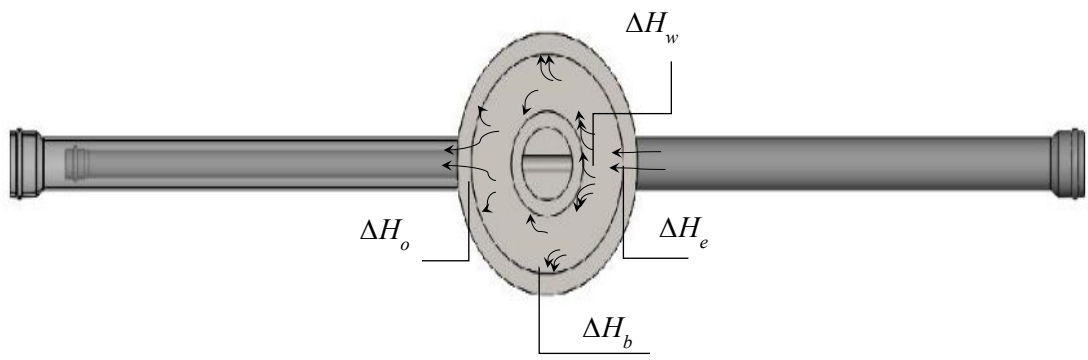


Figure 1 (supplementary) Top view of the new manhole design showing the storm flow path and three points of the head losses generated inside the storm chamber.